# Self-Paced Deep Regression Forests with Consideration on Ranking Fairness

Lili Pan\*, Mingming Meng, Yazhou Ren, Yali Zheng, Zenglin Xu

Abstract-Deep discriminative models (DDMs), e.g. deep regression forests, deep neural decision forests, have been extensively studied recently to solve problems like facial age estimation, head pose estimation, gaze estimation and so forth. Such problems are challenging in part because a large amount of effective training data without noise and bias is often not available. While some progress has been achieved through learning more discriminative features, or reweighting samples, we argue what is more desirable is to learn gradually to discriminate like human beings. Then, we resort to self-paced learning (SPL). But a natural question arises: can self-paced regime lead DDMs to achieve more robust and less biased solutions? A serious problem with SPL, which is firstly discussed by this work, is it tends to aggravate the bias of solutions, especially for obvious imbalanced data. To this end, this paper proposes a new self-paced paradigm for deep discriminative model, which distinguishes noisy and underrepresented examples according to the output likelihood and entropy associated with each example, and tackle the fundamental ranking problem in SPL from a new perspective: fairness. This paradigm is fundamental, and could be easily combined with a variety of DDMs. Extensive experiments on three computer vision tasks, i.e., facial age estimation, head pose estimation and gaze estimation, demonstrate the efficacy of our paradigm. The code in Pytorch is available at https: //github.com/learninginvision/SPU. To the best of our knowledge. our work is the first paper in the literature of SPL that considers ranking fairness for self-paced regime construction.

*Index Terms*—underrepresented examples, ranking fairness, self-paced learning, entropy, deep regression forests.

### I. Introduction

Deep discriminative models (DDMs), which compute the input to output mapping for regression or classification by deep neural networks [1], [2], [3], [4], have recently been applied to many computer vision problems with remarkable success. However, many problems in computer vision are still filled with scenarios in which we require to learn DDMs which is not only robust to noise, but also can conquer imbalanced training data problem [5], [6], [7].

To address these challenges, one common approach is to learn robust and discriminative features through rather deep neural networks, followed by a cost-sensitive discriminative

Lili Pan and Mingming Meng are with the School of Information and Communication Engineering, University of Electronic Science and Technology of China, Chengdu, 611731, and Yangtze Delta Region Institute, University of Electronic Science and Technology of China, Quzhou, 32400, China.

Yazhou Ren is with the School of Computer Science and Engineering, and Yali Zheng is with the School of Automation Engineering, University of Electronic Science and Technology of China, Chengdu, 611731, China.

Zenglin Xu is with the School of Computer Science and Engineering, Harbin Institute of Technology, Shenzhen, and also affiliated with Peng Cheng Lab, Shenzhen, 518055, China.

Under review.

function, often with regularization [8], [9], [10], [5], [11]. The other typical approach is to reweight training samples according to their cost values [12], [13] or gradient directions [14] (*i.e.* meta learning). But, these approaches are not consistent with human cognitive process, as we lean to predict gradually and can distinguish noisy and scarce examples.

This line of thinking force us to resort to self-paced learning—a gradual learning regime inspired by human learning manner. In fact, there are rare studies on the problem of learning DDMs by virtue of self-paced regime. Then, a natural question arises: can self-paced regime guide deep discriminative models to achieve more robust and less biased solutions?

Despite its obvious importance, this issue has not been explored yet. A serious problem associated with SPL, which is firstly discussed by this work, seems to prohibit the forward step. That is existing SPL methods [15], [16], [17], [18] almost assume the training data is balanced, and hence may incur significantly biased solutions when such an assumption fails. The reason lies in the scarce examples, always having *large* loss, would not be selected for training at early paces, as seen in Fig. 1, incurring being ignored. This means the ranking principle in existing SPL methods is unfair to the underrepresented (*i.e.* scarce) examples.

Motivated by this, we propose a new self-paced learning paradigm for DDMs, which tackles the fundamental ranking and selecting problem in SPL from a new perspective—fairness. Specifically, we focus on deep regression forests (DRFs), a typical discriminative model, and propose self-paced deep regression forests with consideration on underrepresented examples (SPUDRFs) for visual mapping problem. The major contributions of this work include:

- By virtue of self-paced regime, we can distinguish confusing and noisy examples from regular ones, and emphasize more on the reliable ones to train DDMs. In addition, we define capped likelihood in SPUDRFs to handle labelling noise for further robustness promotion.
- We define underrepresented examples in SPL, and measure the underrepresented level of each sample by entropy (i.e. predictive uncertainty). Ultimately, we build up a new SPL paradigm: starting with easy and underrepresented examples, as shown in Fig. 1. It could alleviate the bias of final solutions.
- We define fairness metric for regression problem. The results show it can reveal regression fairness with respect to some sensitive features.
- For verification, we apply SPUDRFs on three computer vision problems: (i) facial age estimation, (ii) head pose

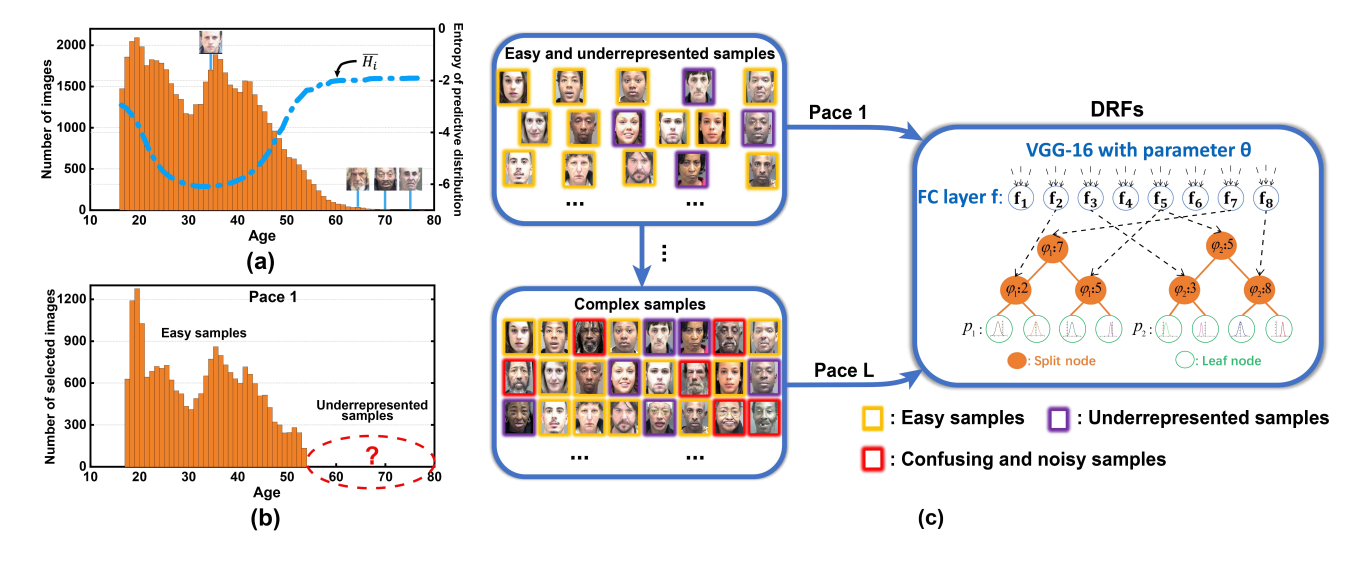


Fig. 1. The Motivation of considering underrepresented examples in DRFs. (a): The histogram shows the number of face images at different ages, and the average entropy curve represents the predictive uncertainty. We observe the high entropy values correspond to *underrepresented examples*. (b): The histogram of the selected face images at pace 1. As the underrepresented examples tend to have relatively large loss, they would not be selected at early pace (*i.e.* ranking unfairness), incurring the final biased solutions. (c): It shows a new self-paced learning paradigm: easy and underrepresented samples first. This builds on the intuition that the underrepresented examples are prone to incur unfair treatment since they are the "minority" in training data.

estimation, and (iii) gaze estimation. Extensive experimental results on the Morph II, FG-NET, BIWI, BU3DFE and MPIIGaze datasets demonstrate the efficacy of our proposed new self-paced paradigm for DDMs. Moreover, on all above tasks, SPUDRFs almost achieve the state-of-the-art performance.

A preliminary version of this work was published in [19]. This paper significantly improves [19] in the following aspects. (i) We extend the model to incorporate capped likelihood, which could promote the robustness further. The robust SPUDRFs can identify and exclude examples with labelling noise, whereas the original is unable, only places more emphasis on reliable one. (ii) We extent the model to integrate with variant weighting schemes; whereas [19] merely adopts mixture weighting scheme. (iii) We define fairness metric for regression in this work, and show obvious fairness improvement of SPUDRFs against the original self-paced deep regression forests (SP-DRFs). (iv) We additionally evaluate SPUDRFs on a new computer vision task, *i.e.*, gaze estimation, and demonstrate its validity on MPIIGaze dataset. (v) Both robustness and fairness evaluation results are added, along with more comprehensive discussions.

This paper is organized as follows. Sec. II introduces related work on SPL, and DDMs for facial age estimation, head pose estimation and gaze estimation. Sec. III details our proposed SPUDRFs. Sec. IV introduces robust SPUDRFs. Sec. V defines fairness metric for regression problem. Sec. VI exhibits and analyzes the experimental results on three computer vision tasks and five related datasets. Sec. VII discusses the strength and potential weakness of this work, followed by Sec. VIII concluding this paper with perspectives.

### II. RELATED WORK

This section reviews self-paced learning methods, as well as the DDMs for facial age estimation, head pose estimation and gaze estimation.

### A. Self-Paced Learning

Self-paced learning is a gradual learning paradigm, which builds on the intuition that, rather than considering all training samples simultaneously, the learning should be presented with the training data from easy to difficult [15], [20]. There exists extensive literature on self-paced learning (SPL). Most of them refers to learning conventional discriminative models through self-paced learning, *e.g.* SVM, logistic regressor. Besides, SPL has also been employed in clustering models recently, such as multi-view clustering [21], [22] and DNNs based clustering [23].

Learning conventional discriminative models by virtue of self-paced regime, exhibit superiority with varying degrees. In [15], Kumar et al. proposed the original SPL framework in that regime suggests processing the samples from an easy to hard order. In [16], Zhao et al. generalized the hard weighting scheme in SPL to soft weighting manner. In [17], Ma et al. proposed self-paced co-training which applies SPL to multi-view or multi-modality problems. In [24], Ren et al. proposed robust softmax regression in which self-paced learning with soft weighting is applied for multi-class classification. In [25], Ren et al. introduced capped-norm into the objective of SPL, so as to further exclude the interference of noisy samples. In fact, the majority of the above works can be cast as incorporating SPL with conventional classifiers, including SVM, logistic regressors and so forth. To learn for regression models, in [26], Han et al. explored to learn mixture of regressors in a self-paced manner, and added  $\ell_{1,2}$  norm regularizer to avoid poorly conditioned linear sub-regressors.

In computer vision, due to the remarkable success of deep neural networks, some authors have realized SPL may guide deep discriminative models to achieve more robust solutions recently. One of the rare works is [18], where Li *et al.* sought to enhance the learning robustness of CNNs by SPL. However, they omitted one important problem in learning discriminative models: the imbalance of training data.

Our work is inspired by the existing works [27], [28] which take the class diversity in sample selection into consideration. Jiang et al. [28] encouraged the class diversity in sample selection at the early paces of self-paced training. Yang et al. [27] defined a metric, named complexity of image category, to measure sample number and classifying difficulty jointly, and introduced such measure in sample selection of SPL. The aforementioned two methods realize, since visual data is often imbalanced, lacking class diversity in sample selection may incur seriously biased solutions; but what cause this has not been mentioned. In this work, we ascertain that the cause of class diversity is exactly ranking unfairness in SPL, where underrepresented examples may often have large loss, particularly in DDMs. Not only that, [27], [28] are only suitable for classification, but not regression in which the output targets are continuous and high dimensional. In this paper, we will go further along this direction, aiming to tackle the fundamental problem in SPL—ranking unfairness.

### B. Facial Age Estimation

Facial age estimation has been actively pursued in the computer vision community for a decade. Recently, along with the rapid development of artificial intelligence, many deep neural networks (DNNs) based approaches [10], [3], [8], [29], [30] have been proposed for age estimation with varying degrees of success. Ordinal-based approaches [10], [3] are the most well known. Niu et al. resorted to a set of sequential binary queries—each query refers to a comparison with a predefined age, to exploit the inter-relationship (ordinal information) among age labels. Furthermore, Gao et al. [8] proposed DLDL-v2 and explored the underlying age distribution patterns to effectively accommodates age ambiguity. Besides, Shen et al. [29] used VGG-16 to extract facial features and modelled the mapping between the extracted features and age by virtue of deep regression forests (DRFs). Li et al. [30] proposed BridgeNet which predicts age by mixing local results. Here, local regressors are learned to partition the data space while gating networks are introduced to provide continuity-aware weights. Deng et al. [31] considered longtailed age classification, and proposed progressive margin loss, where the variational margin is introduced to minimize the influence of head classes that misleads the prediction of tailed samples. Overall, these DDMs based approaches have enhanced age estimation performance significantly; however, they plausibly ignore one problem: the interference arising from confusing and noisy samples-facial images with PIE (i.e. pose, illumination and expression) variation, occlusion, misalignment and so forth. In addition, the imbalanced training data problem is largely ignored.

### C. Head Pose Estimation

Head pose estimation is a long standing problem in computer vision community. Recently, variant DDMs based meth-

ods have been proposed for this problem, boosting pose estimation accuracy dramatically. Of these, Riegler [32] utilized convolutional neural networks (CNNs) to extract patch features within facial images, resulting in more precise results. In [4], Huang et al. proposed multi-modal deep regression networks, with multi-layer perceptron (MLP) architecture, to fuse the RGB and depth images. In [33], Wang et al. proposed a deep coarse-to-fine network for head pose estimation. In [7], Ruiz et al. used a large synthetically expanded head pose dataset to train a rather deep multi-loss convolutional neural networks (CNNs), gaining satisfied accuracy. In [34], Kuhnke et al. proposed domain adaptation for head pose estimation, assuming shared and continuous label spaces. In spite of promoting accuracy, even in the presence of noise, these methods do not clarify how to handle noisy samples explicitly. Moreover, the aforementioned methods seldom mention how to tackle imbalanced training data, which may exactly exist in visual problems.

### D. Gaze Estimation

Appearance-based gaze estimation methods learn a function that maps raw images of eye region or face directly to gaze direction. Recently, several DDMs have been proposed for person-independent gaze estimation. For example, Zhang et al. [35] firstly introduced CNNs into gaze estimation, where LeNet-5 was used, with the result of significantly outperforming conventional approaches, such as random forests. Further, in [36], they employed VGG-16 to encode face image with spatial weights to flexibly suppress or enhance information in different facial regions. In the literature [37], Krafka et al. implemented CNNs-based gaze tracker by processing images from eye regions and the whole face region in a couple manner, taking advantage of both global and local information simultaneously. In [38], Fischer et al. adopted two backbones to extract features from the left and right eye regions separately, and concatenated them to feed into the gaze regression function. Instead of predicting gaze directly, in [39], Park et al. proposed to regress the single eye image to an intermediate pictorial representation, as additional supervision, to simplify 3D gaze direction estimation. Except for person-independent methods, person-specific gaze adaption methods [40], [41], [42] recently have shown potentials of boosting estimation accuracy dramatically, which use a few annotated examples for calibration. Since the ultimate goal of this work is to evaluate the validity of our proposed self-paced regime for DDMs, it only refers to person-independent gaze estimation. Besides, to the best of our knowledge, the existing works seldom discuss whether we should learn DDMs for gaze estimation in a gradual manor, and seldom mention how to handle the interference from illumination, head motion and eye decorations in gaze estimation, as well as imbalanced data problem.

### III. Self-Paced Deep Regression Forests with Consideration on Underrepresented Samples

### A. Preliminaries

In this section, we first review the basic concepts of deep regression forests (DRFs) [29].

Deep Regression Tree. DRFs usually consist of a number of deep regression trees, each of which, given input-output pairs  $\{\mathbf{x}_i, y_i\}_{i=1}^N$ , map extracted features through DNNs to target output by passing a regression tree. Further, a regression tree  $\mathcal{T}$  consists of split (or decision) nodes  $\mathcal{N}$  and leaf (or prediction) nodes  $\mathcal{L}$  [29] (see Fig. 1). Specifically, each split node  $n \in \mathcal{N}$  determines whether a sample  $\mathbf{x}_i$  goes to left or right subtree; each leaf node  $\ell \in \mathcal{L}$  represents a Gaussian distribution  $p_{\ell}(y_i)$  with mean  $\mu_{\ell}$  and variance  $\sigma_{\ell}^2$ —parameters of output distribution defined for each tree  $\mathcal{T}$ .

**Split Node.** Split node represents a split function  $s_n(\mathbf{x}_i; \boldsymbol{\Theta})$ :  $\mathbf{x}_i \to [0,1]$ , where  $\boldsymbol{\Theta}$  denotes the parameters of DNNs, as in Fig. 1(c). Conventionally,  $s_n(\mathbf{x}_i; \boldsymbol{\Theta})$  is formulated as  $\sigma\left(\mathbf{f}_{\varphi(n)}(\mathbf{x}_i; \boldsymbol{\Theta})\right)$ , where  $\sigma(\cdot)$  denotes a sigmoid function while  $\varphi(\cdot)$  denotes an index function specifying the  $\varphi(n)$ -th element of  $\mathbf{f}(\mathbf{x}_i; \boldsymbol{\Theta})$  in correspondence with the split node n, and  $\mathbf{f}(\mathbf{x}_i; \boldsymbol{\Theta})$  denotes the extracted features through DNNs. An example to illustrate the sketch chart of the DRFs is shown in Fig. 1(c), where  $\varphi_1$  and  $\varphi_2$  are two index functions for two trees. Finally, the probability of the sample  $\mathbf{x}_i$  falling into the leaf node  $\ell$  is given by:

$$\omega_{\ell}(\mathbf{x}_{i}|\boldsymbol{\Theta}) = \prod_{n \in \mathcal{N}} s_{n}(\mathbf{x}_{i};\boldsymbol{\Theta})^{[\ell \in \mathcal{L}_{n_{\text{left}}}]} \left(1 - s_{n}(\mathbf{x}_{i};\boldsymbol{\Theta})\right)^{[\ell \in \mathcal{L}_{n_{\text{right}}}]},$$
(1)

where  $[\cdot]$  denotes an indicator function conditioned on the argument. In addition,  $\mathcal{L}_{n_{\text{left}}}$  and  $\mathcal{L}_{n_{\text{right}}}$  correspond to the sets of leaf nodes owned by the sub-trees  $\mathcal{T}_{n_{\text{left}}}$  and  $\mathcal{T}_{n_{\text{right}}}$  rooted at the left and right children  $n_l$  and  $n_r$  of node n.

**Leaf Node.** For a tree  $\mathcal{T}$ , each leaf node  $\ell \in \mathcal{L}$  defines a Gaussian distribution over output  $y_i$  conditioned on  $\{\mu_l, \sigma_l^2\}$ . Since each example  $\mathbf{x}_i$  has the probability  $\omega_\ell(\mathbf{x}_i|\Theta)$  to reach leaf node  $\ell$ , considering all leaf nodes, the predictive distribution over  $y_i$  shall sum all leaf distribution weighted by  $\omega_\ell(\mathbf{x}_i|\Theta)$ :

$$p_{\mathcal{T}}(y_i|\mathbf{x}_i;\mathbf{\Theta}, \boldsymbol{\pi}) = \sum_{\ell \in \mathcal{L}} \omega_{\ell}(\mathbf{x}_i|\mathbf{\Theta}) p_{\ell}(y_i), \tag{2}$$

where  $\pi$  represents the distribution parameters of all leaf nodes associated with tree  $\mathcal{T}$ . Note that  $\pi$  varies along with tree  $\mathcal{T}_k$ , and thus we rewrite them in terms of  $\pi_k$ .

**Forests of Regression Trees.** Since a forest  $\mathcal{F}$  consists of a number of deep regression trees  $\{\mathcal{T}_1,...,\mathcal{T}_k\}$ , the predictive output distribution shall consider all trees:

$$p_{\mathcal{F}}(y_i|\mathbf{x}_i, \mathbf{\Theta}, \mathbf{\Pi}) = \frac{1}{K} \sum_{k=1}^{K} p_{\mathcal{T}_k}(y_i|\mathbf{x}_i; \mathbf{\Theta}, \boldsymbol{\pi}_k), \quad (3)$$

where K is the number of trees and  $\Pi = \{\pi_1, ..., \pi_K\}$ .  $p_{\mathcal{F}}(y_i|\mathbf{x}_i, \boldsymbol{\Theta}, \boldsymbol{\Pi})$  denotes the likelihood that the  $i^{th}$  sample has output  $y_i$ .

### B. Objective

**Underrepresented Examples.** Considering underrepresented examples is the main contribution of this work, it tackles the fundamental ranking and selecting problem in SPL from a new perspective: *fairness*. Here, underrepresented examples mean "minority", as which the examples with similar or the same labels are scarce. Generally, underrepresented examples may

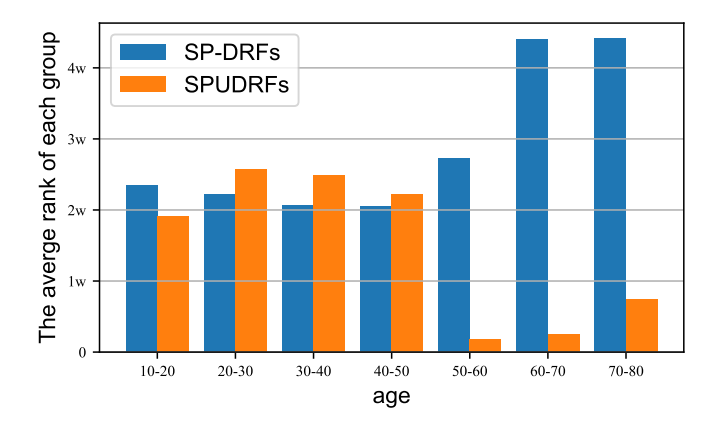


Fig. 2. The average rank of each age group at the first pace of SPL. The ranking results show the original SP-DRFs tends to rank the underrenpresented examples (the elders in MorphII dataset) at the end, probably incurring being ignored at early pace; whereas SPUDRFs rank the underrepresented examples in front to ensure them being selected for training at first.

incur unfairness treatment in early paces due to imbalanced data. The underrepresented level could be measured by predictive uncertainty (*i.e.* entropy).

**Entropy.** Given the sample  $\mathbf{x}_i$ , its predictive uncertainty is formulated as the entropy of  $p_{\mathcal{F}}(y_i|\mathbf{x}_i,\boldsymbol{\Theta},\boldsymbol{\Pi})$ :

$$H\left[p_{\mathcal{F}}\left(y_{i}|\mathbf{x}_{i},\boldsymbol{\Theta},\boldsymbol{\Pi}\right)\right] = \frac{1}{K} \sum_{k=1}^{K} H\left[p_{\mathcal{T}_{k}}\left(y_{i}|\mathbf{x}_{i},\boldsymbol{\Theta},\boldsymbol{\pi}_{k}\right)\right], \quad (4)$$

where  $H\left[\cdot\right]$  denotes entropy, and the entropy which corresponds to the  $k^{th}$  tree is:

$$H\left[p_{\mathcal{T}_{k}}\left(y_{i}|\mathbf{x}_{i},\boldsymbol{\Theta},\boldsymbol{\pi}_{k}\right)\right] = -\int p_{\mathcal{T}_{k}}\left(y_{i}|\mathbf{x}_{i},\boldsymbol{\Theta},\boldsymbol{\pi}_{k}\right)\ln p_{\mathcal{T}_{k}}\left(y_{i}|\mathbf{x}_{i},\boldsymbol{\Theta},\boldsymbol{\pi}_{k}\right)dy_{i}.$$
(5)

The large the entropy is, the more uncertain the prediction should be, *i.e.*, the more underrepresented the sample is.

The predictive distribution  $p_{\mathcal{T}_k}\left(y_i|\mathbf{x}_i;\boldsymbol{\Theta},\boldsymbol{\pi}_k\right)$  takes the form  $\sum_{\ell\in\mathcal{L}}\omega_\ell(\mathbf{x}_i|\boldsymbol{\Theta})p_\ell(y_i)$ . The integral of mixture of Gaussians in Eq. (5) is non-trivial. Monte Carlo sampling can address this, but incurs large computational cost [43]. Here, we use the lower bound of this integral to approximate the true value:

$$H\left[p_{\mathcal{T}_k}\left(y_i|\mathbf{x}_i,\boldsymbol{\Theta},\boldsymbol{\pi}_k\right)\right] \approx \frac{1}{2} \sum_{\ell \in \mathcal{L}} \omega_{\ell}(\mathbf{x}_i|\boldsymbol{\Theta}) \left[\ln\left(2\pi\sigma_{\ell}^2\right) + 1\right].$$
(6)

**Formulation.** Let  $v_i$  be a latent variable indicating whether the  $i^{th}$  sample is selected  $(v_i=1)$  or not  $(v_i=0)$  for training. Our objective is to jointly maximize the log likelihood function with respect to DRFs' parameters  $\boldsymbol{\Theta}$  and  $\boldsymbol{\Pi}$ , and learn the latent variables  $\mathbf{v}=(v_1,...,v_N)^T$ . Fig.2 shows the original self-paced regime may not select the underrepresented examples in early pace, incurring ignorance of them. Considering fairness, we prefer to select the underrepresented examples, which probably have higher predictive uncertainty (i.e. entropy), particularly in early pace. Therefore, we maximize the

likelihood function of DRFs coupled with sample selection term, meanwhile considering ranking fairness,

$$\max_{\mathbf{\Theta}, \mathbf{\Pi}, \mathbf{v}} \sum_{i=1}^{N} v_i \left\{ \log p_{\mathcal{F}} \left( y_i | \mathbf{x}_i, \mathbf{\Theta}, \mathbf{\Pi} \right) + \gamma H_i \right\} + \lambda \sum_{i=1}^{N} v_i, \quad (7)$$

where  $\lambda$  is a parameter controlling the learning pace  $(\lambda \geq 0)$ ,  $\gamma$  is the parameters imposing on uncertainty  $(\lambda \geq 0)$ , and  $H_i$  denotes the entropy of the predictive distribution associated with the  $i^{th}$  sample. When  $\gamma$  decays to 0, the objective function is equivalent to the log likelihood function with respect to DRFs' parameters  $\Theta$  and  $\Pi$ . Eq. (7) indicates each sample is weighted by  $v_i$ , and whether  $\log p_{\mathcal{F}}(y_i|\mathbf{x}_i,\Theta,\Pi)+\gamma H_i>-\lambda$  determines the  $i^{th}$  sample is selected or not. That is, the sample with high likelihood value or entropy may be selected. The optimal  $v_i^*$  is:

$$v_i^* = \begin{cases} 1 & \text{if } \log p_{\mathcal{F}_i} + \gamma H_i > -\lambda \\ 0 & \text{otherwise} \end{cases}, \tag{8}$$

where  $p_{\mathcal{F}}(y_i|\mathbf{x}_i, \boldsymbol{\Theta}, \boldsymbol{\Pi})$  is denoted by  $p_{\mathcal{F}i}$  for simplicity, and we use this representation in all following parts. Iteratively increasing  $\lambda$  and decreasing  $\gamma$ , samples are dynamically involved in the training of DRFs, starting with easy and underrepresented examples and ending up with all samples. Thus, SPUDRFs are prone to achieve more robust and less biased solutions.

One might argue that the noisy and hard examples tend to have high predictive uncertainty, rendering being selected in the early pace. In fact, from Eq. (8), we observe whether one sample is selected is determined by both its predictive uncertainty and the log likelihood of being predicted correctly. The noisy and hard samples probably have relatively large loss i.e. low log likelihood  $\log p_{\mathcal{F}i}$ , and would not be selected at the very start.

### C. Weighting Strategies

Weighting each sample on the basis of its importance would be more precise in SPUDRFs. In the previous section, we adopt a hard weighting scheme in SPUSRFs as described in Eq. (7), where one sample either selected or not is determined by  $v_i$ . Such a weighting scheme appears to omit the importance of each sample. In fact, SPUDRFs can easily be incorporated with other weighting schemes, including: mixture weighting and soft weighting [44].

**Mixture Weighting.** Mixture weighting scheme [44] weights selected sample by its importance, *i.e.*,  $0 \le v_i \le 1$ . The objective function with mixture weighting is defined as:

$$\max_{\mathbf{\Theta}, \mathbf{\Pi}, \mathbf{v}} \sum_{i=1}^{N} v_i \left\{ \log p_{\mathcal{F}_i} + \gamma H_i \right\} + \zeta \sum_{i=1}^{N} \log \left( v_i + \zeta / \lambda \right), \quad (9)$$

where  $\zeta$  is a parameter controlling the learning pace. We set  $\zeta = \left(\frac{1}{\lambda'} - \frac{1}{\lambda}\right)^{-1}$ , and  $\lambda > \lambda' > 0$  to construct a reasonable soft weighting formulation. The self-paced regularizer in Eq. (9) is convex with respect to  $v \in [0,1]$ . Then, setting the partial gradient of Eq. (9) with respect to  $v_i$  to be zero will lead the following:

$$\log p_{\mathcal{F}i} + \gamma H_i + \frac{\zeta}{v_i + \zeta/\lambda} = 0. \tag{10}$$

The optimal solution of  $v_i$  is given by:

$$v_{i}^{*} = \begin{cases} 1 & \text{if } \log p_{\mathcal{F}i} + \gamma H_{i} \geq -\lambda' \\ 0 & \text{if } \log p_{\mathcal{F}i} + \gamma H_{i} \leq -\lambda \\ \frac{-\zeta}{\log p_{\mathcal{F}i} + \gamma H_{i}} - \zeta/\lambda & \text{otherwise} \end{cases}$$
(11)

If either the log likelihood or the entropy is too large,  $v_i^*$  equals to 1. In addition, if the likelihood and entropy are both too small,  $v_i^*$  equals to 0. Except the above two situations, the soft weighting, *i.e.*, the last line of Eq. (11), is adopted.

**Soft Weighting.** Soft weighting scheme [44] weights selected sample with respect to its output likelihood and entropy. It includes: linear scheme and logarithmic scheme.

**Linear scheme.** It linearly assigns weight to sample with respect to its output likelihood and entropy. The objective is formulated as:

$$\max_{\mathbf{\Theta}, \mathbf{\Pi}, \mathbf{v}} \sum_{i=1}^{N} v_i \{ \log p_{\mathcal{F}i} + \gamma H_i \} - \frac{1}{2} \lambda \sum_{i=1}^{N} \left( v_i^2 - 2v_i \right), \quad (12)$$

where  $\lambda > 0$ ,  $v_i \in [0, 1]$ . We set the partial gradient of Eq. (12) with respect to  $v_i$  as zero, and the optimal solution for  $v_i$  is:

$$v_i^* = \begin{cases} \frac{\log p_{\mathcal{F}_i} + \gamma H_i + \lambda}{\lambda} & \text{if } \log p_{\mathcal{F}_i} + \gamma H_i \ge -\lambda \\ 0 & \text{otherwise} \end{cases}$$
 (13)

The larger the log likelihood and entropy, the higher the weight should be.

**Logarithmic scheme.** It penalizes the output likelihood and entropy logarithmically, which can be achieved by the following objective function:

$$\max_{\mathbf{\Theta}, \mathbf{\Pi}, \mathbf{v}} \sum_{i=1}^{N} v_i \left\{ \log p_{\mathcal{F}i} + \gamma H_i \right\} - \sum_{i=1}^{N} \left( \zeta v_i - \frac{\zeta^{v_i}}{\log \zeta} \right), \quad (14)$$

where  $\zeta = 1 - \lambda$ ,  $0 < \lambda < 1$  and  $v_i \in [0, 1]$ . Similarly, the optimal solution of  $v_i$  can be obtained:

$$v_i^* = \begin{cases} \frac{\log(\zeta - \log p_{\mathcal{F}_i} - \gamma H_i)}{\log \zeta} & \text{if } \log p_{\mathcal{F}_i} + \gamma H_i \ge -\lambda \\ 0 & \text{otherwise} \end{cases} . \tag{15}$$

### D. Underrepresented Example Augmentation

As previously mentioned, SPUDRFs emphasize more on underrepresented examples, rendering less biased solutions. Since the intrinsic reason that leads to biased solutions plausibly is the imbalanced training data, we further re-balance data distribution via a curriculum reconstruction strategy. More specifically, we distinguish the underrepresented examples, whose  $H_i$  is larger than  $\beta$ , from regular ones at each pace, and augment them into the training data. Since the number of underrepresented examples increases through augmentation, the data distribution bias is alleviated.

### E. Optimization

We propose a two-step alternative search strategy (ASS) algorithm to solve Eq. (7): (i) update  $\mathbf{v}$  for sample selection with fixed  $\mathbf{\Theta}$  and  $\mathbf{\Pi}$ , and (ii) update  $\mathbf{\Theta}$  and  $\mathbf{\Pi}$  with current fixed sample weights  $\mathbf{v}$ . With fixed  $\mathbf{v}$ , our DRFs is learned by alternatively updating  $\mathbf{\Theta}$  and  $\mathbf{\Pi}$ . In [29], the parameters  $\mathbf{\Theta}$ 

### Algorithm 1 The training process of SPUDRFs.

```
Input: \mathcal{D} = \{\mathbf{x}_i, \mathbf{y}_i\}_{i=1}^N. Output: Model parameters \Pi, \Theta.
 1: Initialize \Pi^0, \Theta^0, \lambda^0, \gamma^0.
2: while not converged do
        Update \mathbf{v} by Eq. (8).
           while not converged do
4:
                  Randomly select a mini-batch from \mathcal{D}.
 5:
                  Calculate H_i for each sample by Eq. (5).
 6:
                  Update \Theta and \Pi to maximize Eq. (7).
 7:
           end while
8:
           Increase \lambda and decrease \gamma.
10: end while
```

for split nodes (*i.e.* parameters for VGG) is updated through gradient descent since the loss is differentiable with respect to  $\Theta$ . While the parameters  $\Pi$  for leaf nodes are updated by virtue of variational bounding [29] when fixing  $\Theta$ .

## IV. ROBUST SELF-PACED DEEP REGRESSION FORESTS WITH CONSIDERATION ON UNDERREPRESENTED EXAMPLES

In the previous section, we have discussed self-paced regime tends to emphasize reliable samples. However, it does not have the capability of excluding noisy samples, especially labelling noise. To fix this drawback, this work constructs capped-likelihood function in SPUDRFs. Specifically, it renders the output likelihood with especially small value to zero:

$$cap(p_{\mathcal{F}i}, \epsilon) = \frac{\max(p_{\mathcal{F}i} - \epsilon, 0)}{p_{\mathcal{F}i} - \epsilon} p_{\mathcal{F}i}, \tag{16}$$

where  $\epsilon$  denotes the threshold and  $\epsilon > 0$ . Given the output likelihood  $p_{\mathcal{F}_i}$ , the capped likelihood  $p_{\mathcal{F}_i}^c = \text{cap}\,(p_{\mathcal{F}_i},\epsilon)$ . As the log likelihood of the noisy samples are prone to have especially small values, such an operation sets them to be  $-\infty$ . Thus, incorporating capped likelihood into SPUDRFs potentially avoids the interference of noisy, especially labelling noise:

$$\max_{\mathbf{\Theta}, \mathbf{\Pi}, \mathbf{v}} \sum_{i=1}^{N} v_i \left\{ \log p_{\mathcal{F}_i}^c + \gamma H_i \right\} + \lambda \sum_{i=1}^{N} v_i, \tag{17}$$

The robust SPUDRFs can be optimized using the optimization method proposed in Sec. III-E. One note if  $p_{\mathcal{F}_i} \leq \epsilon$ , the capped likelihood  $p_{\mathcal{F}_i}^c = 0$ , that is  $\log p_{\mathcal{F}_i}^c = -\infty$ . Since  $\lambda$  is a positive factor, maximizing Eq. (17) must yields  $v_i = 0$ , meaning the  $i^{th}$  sample would not be selected. By adjusting  $\epsilon$ , we can exclude a certain ratio of noise samples to obtain a more robust model.

### V. FAIRNESS METRIC

Except accuracy, fairness should also be an important metric to measure the performance of a regression model, particularly when the regression targets are related to sensitive attributes. For example, in age estimation, we expect our model to treat the younger and the elder fairly, *i.e.*, not large MAEs for the former, but small MAEs for the latter.

The notion of fairness is originally defined with respect to a protected attribute such as gender, race or age. In fact, the term fairness has a range of potential definitions, here, we here adopt the notion of fairness that is with respect to sensitive features [45]. Defining fairness metric for regression is one of the contributions of this work.

There exists some works [46], [47], [48], [49] about fairness constraints in regression, for example, statistical parity, bounded group loss [46], [48], but seldom refers to fairness metrics. Thus, in this work, we formulate fairness metric for regression. Specifically, we divide the test dataset into K subsets, each of which is denoted by  $\mathbf{D}_k = \{\mathbf{x}_i, y_i | y_i \in \mathcal{G}_k\}$ , and  $\mathcal{G}_k$  denotes the  $k^{th}$  group. A fair model is expected to show the same performance on all subsets, which can be formulated as:

$$\mathbb{E}_{k}\left[L\left(\hat{y},y\right)\right] = \mathbb{E}_{l}\left[L\left(\hat{y},y\right)\right] \quad \forall k,l \in \left\{1,2,...,K\right\}, k \neq l.$$
(18)

where  $\mathbb{E}_k[\cdot]$  denotes an expectation with respect to the loss  $L(\cdot)$  over group  $\mathbf{D}_k$ ,  $\hat{y}$  is the predicted value of the model and y is the real target value. Motivated by p%-rule [49], which measure classification fairness, we evaluate fairness between two subsets  $\mathbf{D}_k$  and  $\mathbf{D}_l$  as follows:

$$f\left(\mathbf{D}_{k}, \mathbf{D}_{l}\right) = \min\left(\frac{\mathbb{E}_{k}\left[L\left(\hat{y}, y\right)\right]}{\mathbb{E}_{l}\left[L\left(\hat{y}, y\right)\right]}, \frac{\mathbb{E}_{l}\left[L\left(\hat{y}, y\right)\right]}{\mathbb{E}_{k}\left[L\left(\hat{y}, y\right)\right]}\right). \tag{19}$$

The ratio of loss expectation characterizes the fairness of the model on every two subsets. Small ratio means the performance on such two subsets is very different, reflecting model bias against a certain subset. On the contrary, a large ratio indicates the losses on  $\mathbf{D}_k$  and  $\mathbf{D}_l$  are similar, revealing the model is relatively fair to  $\mathbf{D}_k$  and  $\mathbf{D}_l$ . Particularly, when the ratio is equal to 1, the model satisfies Eq. (18), and  $\mathbf{D}_k$  and  $\mathbf{D}_l$  are treated fairly.

The regression fairness, in this paper, is define as the expectation of Eq. (19), which considers the fairness between any two subsets,

$$FAIR = \mathbb{E}\left[f\left(\mathbf{D}_{i}, \mathbf{D}_{i}\right)\right]. \tag{20}$$

In SPUDRFs, when we set  $\gamma>0$ , all samples are sorted by both likelihood and entropy, so easy and underrepresented ones are selected equally, which means samples from all subsets will be selected at early paces. Therefore, our model can alleviate the model's prejudice against different subsets and improve regression fairness. More extensive evaluation results can be found in Sec. VI-F.

### VI. EXPERIMENTAL RESULTS

### A. Datasets and Experimental Setup

**Dataset.** There are 5 datasets used in our experiments, namely Morph II, FG-NET, BIWI, BU3DFE and MPIIGaze.

**Morph II.** The Morph II [50] dataset contains 55,134 face images of 13618 individuals with unbalanced gender and ethnicity distributions. These images are near-frontal pose, neutral expression, and uniform illumination.

**FG-NET.**The FG-NET [51] dataset includes 1,002 color and grey images of 82 people with each subject having more than 10 photos at different ages. Since all images were taken in a

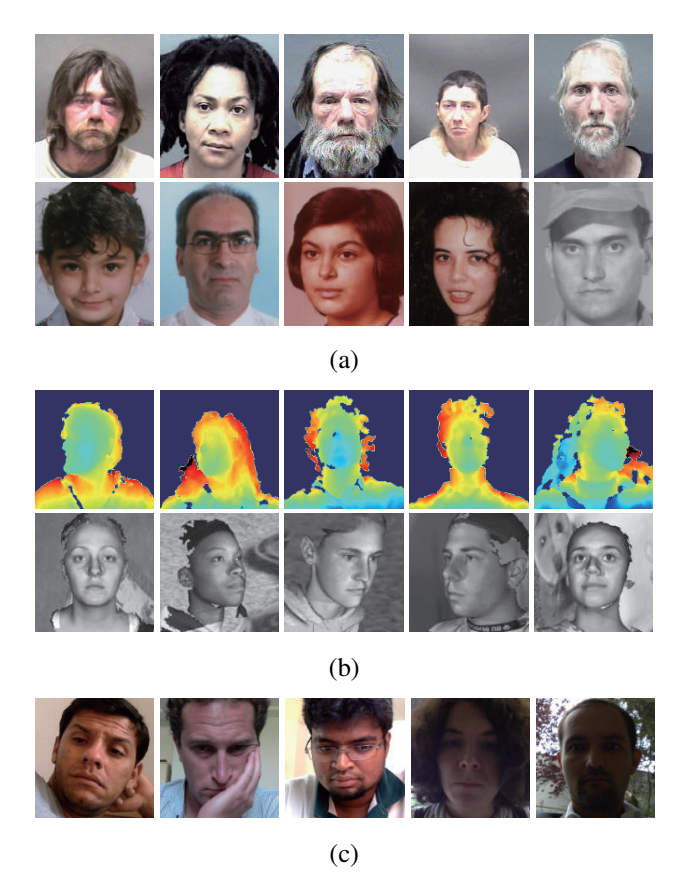


Fig. 3. Some example images in II, FG-NET, BIWI, BU3DFE and MPIIGaze datasets. (a) **Age:** the images in the first row is from the Morph II dataset, while the images in the second row is from the FG-NET dataset. (b) **Pose:** the images in the first row is from the BIWI head pose dataset, while the images in the second row is from the BU3DFE dataset. (c) **Gzae:** The example images in MPIIGaze dataset.

totally uncontrolled environment, there exisits a large deviation on lighting, pose and expression (*i.e.* PIE) of faces inside the dataset.

**BIWI.** The BIWI dataset [52] includes 15678 images collected by a Kinect sensor device for different persons and head poses with pitch, yaw and roll angles mainly ranging within  $\pm 60^{\circ}$ ,  $\pm 75^{\circ}$  and  $\pm 50^{\circ}$ . These images are from 20 subjects, including 10 males and 6 females, where 4 males have been captured twice with/without glasses.

**BU3DFE.** The BU-3DFE dataset [53] is collected from 100 subjects of which 44 are male and 56 are female. Following the work [53], we randomly rotated the 3D face models to produce 6000 images with pitch and yaw angles ranging within  $\pm 30^{\circ}$  and  $\pm 90^{\circ}$ .

**MPIIGaze.** The MPIIGaze dataset [35] includes 213659 images from 15 persons. The number of images for each person is between 1498 and 34745. The normalized gaze angle is in the range of  $[-20^{\circ}, +5.0^{\circ}]$  degrees in vertical and  $[-25^{\circ}, +25^{\circ}]$  degrees in horizontal. Due to huge deviation of image number amongst different persons, similar to [35], we used 1500 images from left and right eyes of each person.

**Reprocessing and Data Augmentation.** MTCNN [54] was used for joint face detection and alignment on the Morph II and FG-NET datasets. Besides, following [29], two ways

of augmentation: 1) random cropping; 2) random horizontal flipping were adopted for data augmentation. On BIWI and BU3DFE, only random cropping was adopted for augmentation. On MPIIGaze, two normalized eye images (*i.e.* left and right) were obtained following the work [35], and only random cropping was used for data augmentation.

Parameter Setting. The VGG-16 [55] was employed as the fundamental backbone networks of SPUDRFs. Following [38], on MPIIGaze dataset two VGG-16 networks were used for left and right eyes separately. The hyper-parameters of VGG-16 were: training batch size (32 on Morph II, BIWI and BU3DFE, 8 on FGNET, 128 on MPIIGaze), drop out ratio (0.5), max iterations of each pace (80k on Morph II, 10k on FGNET, 20k on BIWI and BU3DFE, 5k on MPIIGaze), SGD optimizer on BIWI and Adam optimizer on other datasets, initial learning rate  $(2 \times 10^{-5})$  on Morph II and BU3DFE,  $1 \times 10^{-5}$  on FG-NET, 0.2 on BIWI,  $3 \times 10^{-5}$  on MPIIGaze) by reducing the learning rate (0.5) per 10k iterations. Here, some hyper-parameters are slightly different to the settings in the previous Caffe version [19]. In addition, the pre-trained model was VGG-Face [9] for Morph II, BIWI, FG-NET, and VGG-16 pre-trained on IMDB-WIKI [5] for FG-NET, as well as VGG-16 for MPIIGaze.

The hyper-parameters of SPUDRFs were: tree number (5), tree depth (6), output unit number of feature learning (128), iterations to update leaf node predictions (20), number of images to update leaf node predictions (the whole training set on MPIIGaze and 50 times of batch size on other datasets). In the first pace, 50% samples which are easy or underrepresented were selected for training. Here,  $\lambda$  was set to guarantee the first 50% samples with large  $\log p_{\mathcal{F}i} + \gamma H_i$  values were involved.  $\lambda'$ was set to ensure 10% selected samples adopt soft weighting when adopting mixture weighing scheme. To further promote efficiency, we preserved the selected samples in previous pace and rank the rest samples in current pace for sample selection.  $\gamma$  was initialized to be 15 on the Morph II and BIWI datasets, and 5 on the FG-NET, BU-3DFE and MPIIGaze dataset.  $\beta$ was set to distinguish a certain number of samples as the ones need to be augmented twice at each pace (1000 on BIWI, 400 on BU3DFE, 2000 on MPIIGaze). The number of paces was empirically set to be 10 on the Morph II, 6 on the BIWI and MPIIGaze, 3 on the FG-NET and BU-3DFE datasets. Except the first pace, equal proportion of the rest data was gradually involved at each pace.

**Evaluation Details.** To evaluate regression accuracy, we use the mean absolute error (MAE):  $\sum_{i=1}^{N} |\hat{y}_i - y_i|/N$ , where  $\hat{y}_i$  represents the predicted output for the  $i^{th}$  sample, and N is the total number of images for testing. In addition, cumulative score (CS) is defined in age estimation, which calculates the percentage of images sorted in the range of  $[y_i - L, y_i + L]$ :  $CS(L) = \sum_{i=1}^{N} [|\hat{y}_i - y_i| \le L]/N \cdot 100\%$ , where  $[\cdot]$  denotes an indicator function and L is the error level. Further, to measure regression fairness, we adopt our proposed fairness metric FAIR given in Sec.V.

To calculate the above metrics, on Morph II, BIWI and BU3DFE, the dataset was divided into two sets: 80% for training and the rest 20% for testing. The random division was repeated 5 times and the reported performance was averaged

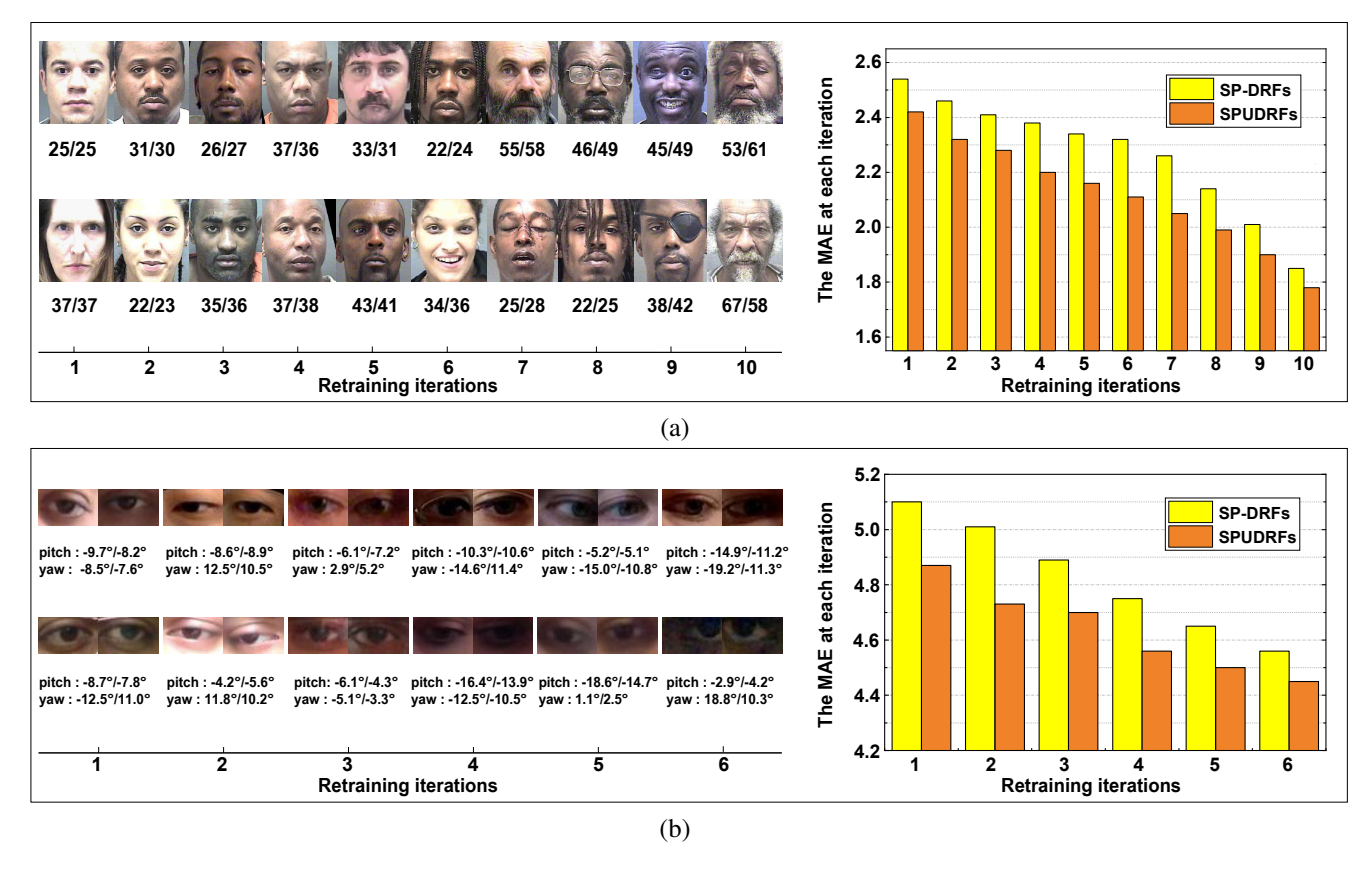


Fig. 4. The gradual learning process of SP-DRFs and SPUDRFs on Morph II (a) and MPIIGaze (b). Left: The typical worst cases at each iteration become more confusing and noisy along with iteratively increasing  $\lambda$  and decreasing  $\gamma$ . The two numbers below each image are the real labels (left) and predicted targets (right). Right: The MAEs of SP-DRFs and SPUDRFs at each pace descends gradually. The SPUDRFs show its superiority of taking predictive uncertainty into consideration, when compared with SP-DRFs.

over 5 times. The leave-one-person-out protocol was used on FG-NET [29] and MPIIGaze [35], where one subject was used for testing and the remaining subjects for training.

### B. Validity of SP-DRFs

This section studies the validity of learning DDMs by virtue of self-paced regime with consideration on ranking fairness. **Self-Paced Learning Strategy.** Fig. 4(a) illustrates the representative face images at each learning pace of SPUDRFs, along with increasing  $\lambda$  and decreasing  $\gamma$ . The two numbers below each image are the real age (left) and predicted age (right). We observe that the training images in the later paces are obviously more confusing and noisy than the ones in the early paces. Since our model is initialized by the results of the last retraining pace, meaning adaptively calibrated by "good" samples rather than confusing and noisy ones. As a result, it has improved performance compared with DRFs, where the MAE is promoted from 2.17 to 1.78, and the CS is improved from 91.3% to 93.34% (see Fig. 6(a)).

Fig. 4(b) shows the representative gaze images at each learning pace of SPUDRFs. The two numbers below each pair of images are the real gaze direction (left) and predicted gaze direction (right). The same phenomena—the easy examples are selected in the early paces while confusing and noisy ones are selected in the later paces—can be observed on

the MPIIGaze datasets. Meanwhile, the MAEs at each pace gradually decrease, and finally decrease to 4.45, where DRFs have a MAE of 4.62 (see Table. II).

Considering Ranking Fairness. Fig. 5 visualizes the leaf node distributions of SP-DRFs and SPUDRFs in the progressive learning. The Gaussian means  $\mu_l$  associated with the 160 leaf nodes, where each 32 leaf nodes are defined for 5 trees, are plotted in each sub-figures. Three paces, *i.e.* pace 1, 3, and 6, are randomly chosen for visualization. Only pitch and yaw angles are shown for clarity. Besides, the original distribution of pitch and yaw angles associated with all images in BIWI are also shown.

In Fig. 5, the comparison results between SP-DRFs and SPUDRFs demonstrate the efficacy of considering ranking fairness in SPL. For SP-DRFs, where ranking fairness has not been considered, the Gaussian means of leaf nodes (red points in the second row) are concentrated in a small range, incurring seriously biased solutions. That means the underrepresented examples have not been treated fairly. The poor MAEs are the evidence for this, which are great inferior to SPUDRFs (see Tab. II). SPUDRFs rank samples by log likelihood coupled with entropy (*i.e.* more fair), and are prone to achieve less unbiased/unfair solutions, as shown in the third rows of Fig. 5.

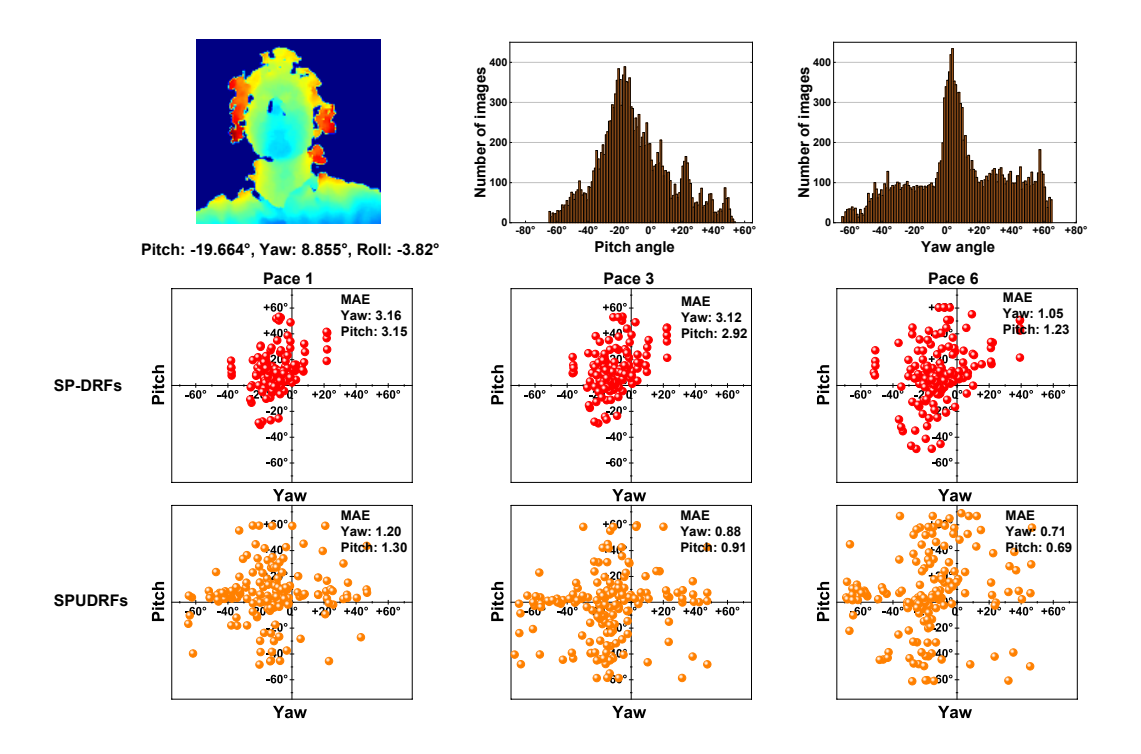


Fig. 5. The leaf node distribution of SP-DRFs and SPUDRFs in gradual learning process. Three paces, *i.e.* pace 1, 3, and 6, are randomly chosen for visualization. For SP-DRFs, the Gaussian means of leaf nodes (the red points in the second row) are concentrated in a small range, incurring seriously biased solutions. For SPUDRFs, the Gaussian means of leaf nodes (the orange points in the third row) distribute widely, leading to much better MAE performance.

### C. Comparison with State-of-the-art Methods

We compare SPUDRFs with other state-of-the-art methods on three vision tasks, age estimation, head pose estimation and gaze estimation.

Results on Age Estimation. The comparison between SPU-DRFs and other baseline methods on Morph II and FG-NET are shown in Fig. 6. The baseline methods include: LSVR [56], RCCA [57], OHRank [58], OR-CNN [10], Ranking-CNN [3], DRFs [29], DLDL-v2 [8], and PML [31]. The results show some consistent trends. Firstly, owing to DNNs, SPUDRFs have superior performance to conventional discriminative models, such as LSVR [56] and OHRank [58]. Secondly, due to the self-paced regime, SPUDRFs outperform other DDMs, thereby leading to more robust and less biased solutions. Thirdly, SPUDRFs outperform SP-DRFs on both MAE and CS, and almost achieve state-of-the-art performance. Fig. 6(b) shows the CS comparison on this dataset. We observe the CS of SPUDRFs reach 93.34% at error level L=5, significantly outperforming DRFs by 2.04%. Fig. 7(a) shows the comparison results of SPUDRFs with the stateof-the-art approaches on FG-NE, where SPUDRFs reach an MAE of 2.64, outperforming DRFs by 0.16. Besides, the CS comparisons are shown in Fig. 7(b), SPUDRFs consistently outperform other recent proposed methods.

**Results on Head Pose Estimation.** Tab. I shows the comparison results of our methods with several recent head pose estimation approaches. SVR [64], RRF [65] and KPLS [66]

Method	MAE↓	CS↑
LSVR [56]	4.31	66.2%
RCCA [57]	4.25	71.2%
OHRank [58]	3.82	N/A
OR-CNN [10]	3.27	73.0%
Ranking-CNN [3]	2.96	85.0%
DLDL-v2 [8]	1.97	N/A
DRFs [29]	2.17	91.3%
PML [31]	2.15	N/A
SP-DRFs	1.84 <sup>1</sup>	92.85%
SPUDRFs	1.78	93.34%

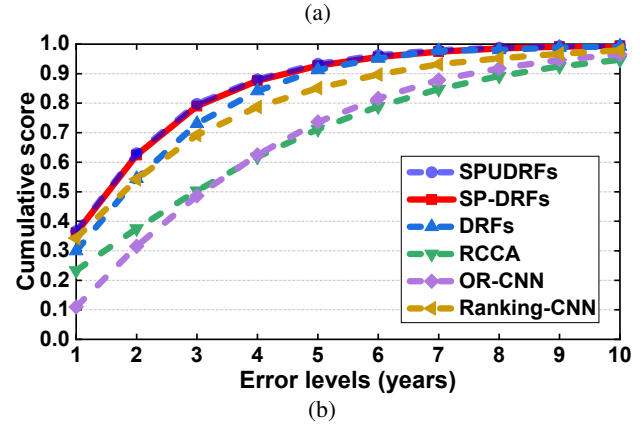


Fig. 6. The comparison results on the Morph II dataset: (a) The MAE comparison with the state-of-the-art methods, (b) the CS curves of the comparison methods.

are all conventional regression methods, and hence have inferior performance to MoDRN. SPUDRFs achieve the best performance with an MAE of 0.74 on the BIWI dataset and

<sup>&</sup>lt;sup>1</sup>The MAE and CS results reported in the current version are slightly different to our previous work [19] because we used Pytorch currently but Caffe previously.

MAE↓	CS↑
5.77	N/A
5.07	68.9%
4.83	72.3%
4.80	74.3%
4.48	74.4%
4.12	73.5%
2.80	84.50%
2.68 <sup>1</sup>	87.41%
2.64	88.59%
	5.77 5.07 4.83 4.80 4.48 4.12 2.80 <b>2.68</b> <sup>1</sup>

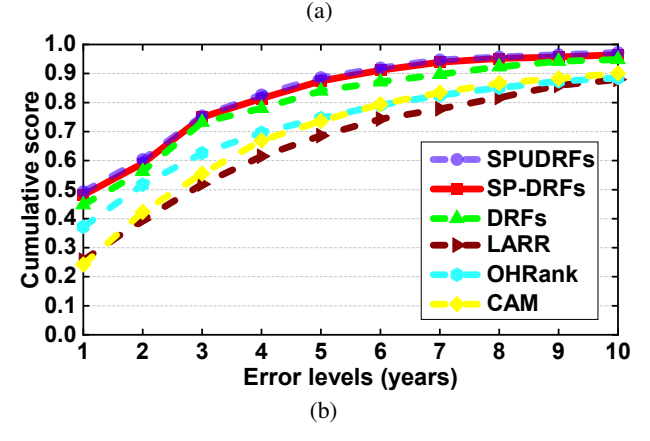


Fig. 7. The comparison results on the FG-NET dataset: (a) The MAE comparison with the state-of-the-art methods, (b) the CS curves of the comparison methods.

0.82 on the BU-3DFE dataset, which is state-of-the-art. Such an obvious promotion, from 1.13 to 0.74 on BIWI, should owe to considering ranking fairness in the initial stage of training DRFs. *The importance of considering ranking fairness in SPL is most obvious on BIWI*. In SP-DRFs, as illustrated in Fig. 5, the Gaussian means of leaf nodes are concentrated in a small range, leading biased solutions. In SPUDRFs, considering underrepresented examples in the early pace renders more reasonable distributions of leaf nodes.

Method	MAE↓	Method	MAE↓		
SVR [64]	3.14	SVR [64]	4.21		
RRF [65]	3.06	SAE [67]	4.14		
KPLS [66]	2.88	KPLS [66]	4.12		
SAE [67]	1.94	RRF [65]	4.09		
MoDRN [4]	1.62	MoDRN [4]	3.86		
DRFs [29]	$1.33^{2}$	DRFs [29]	0.99		
SP-DRFs	1.13	SP-DRFs	0.89		
<b>SPUDRFs</b>	0.74	SPU-DRFs	0.82		
(a) (b)					
TABLE I					

THE COMPARISON WITH STATE-OF-THE-ART METHODS: (A) THE BIWI DATASET, (B) THE BU-3DFE DATASET.

Results on Gaze Estimation. Tab. II shows the gaze estimation results of our methods and others on the MPIIGaze dataset. Both mean error across all participants and standard deviation across persons are reported. The standard deviation of RT-GENE [38], Pict-Gaze [39], Ordinal Loss [68] are not reported because the original works do not provide. SPUDRFs outperforms all baseline methods in MAE, confirming the

effectiveness of our learning regime. RT-GENE [38] adopts additional image augmentation, and uses the feature extracted via VGG-16 to regress for gaze directly, while DRFs introduce random forest as regression function. Hence, RT-GENE has inferior MAE to DRFs (4.80 against 4.62). Pict-Gaze [39] uses gaze map as additional supervision, and Ordinal [68] utilizes ordinal loss with order regularization to solve regression problem, but both of them ignore the differences between samples and train all samples at the same time. SPUDRFs prioritize easy and underrepresented samples, then confusing and noisy ones. The MAE of [39] and [68] are 4.56 and 4.49 respectively, and our method is 4.45, which achieves the best performance. It's noteworthy the phenomenon that SP-DRFs only promote the gaze estimation performance slightly when compared with DRFs, we speculate this is due to the heterogeneous data distribution between training set and test set in leave-one-out setting.

Method	MAE↓				
MPIIGaze [35]	$6.30\pm1.80$				
iTracker [37]	$6.20 \pm 0.85$				
GazeNet+ [69]	$5.40 \pm 0.67$				
MeNets [70]	$4.90 \pm 0.59$				
RT-GENE [38]	$4.80 \pm$				
Pict-Gaze [39]	$4.56 \pm$				
Ordinal Loss [68]	$4.49 \pm$				
DRFs [29]	$4.62 \pm 0.89$				
SP-DRFs	$4.57 \pm 0.78$				
SPU-DRFs	$4.45 \pm 0.84$				
TABLE II					

The comparison with state-of-the-art methods on the  $\mathbf{MPIIG} \mathbf{Aze} \ \mathbf{DATASET}.$ 

### D. Different Weighting Schemes

Variant weighting schemes in SUPDRFs are compared on different tasks and datasets, as shown in Table. III. The performances of different schemes are only slightly different. We observe the weights for most samples are close to 1, and only a small number of samples (the most under the Log weighting scheme, only 2%) have weights below 0.5. Hence, the MAEs with different weighting schemes are very close, with only minor difference, which is reasonable. Even with different weighting schemes, we observe SPUDRFs always outperform SP-DRFs. Especially on BIWI, the best MAE for SP-DRFs with different weighting schemes is 1.13 and the best for SPUDRFs is 0.74. The reason has been discussed previously, that is SPUDRFs consider ranking fairness and are prone to achieve less biased solutions.

### E. Robust SPUDRFs

To test the validity of robust SPUDRFs, which has the capability to hand labelling noise, we manually added Gaussian noise to the labels on the Morph II, BIWI and MPIIGaze datasets. Specially, 10% samples were randomly chosen in each of the above dataset, and their labels were disturbed by Gaussian noise with mean 0 and standard deviation 10.  $\epsilon$  was appropriately set to be variant values, controlling the proportion (from 0% to 20%) of samples whose likelihood is capped to 0, i.e., the portion of samples to be excluded.

<sup>&</sup>lt;sup>2</sup>The reported results are better than our previous work [19] because we used floating point label in our current experiment but integral label in [19].

TABLE III

RESULTS OF OUR PROPOSED METHODS WITH DIFFERENT WEIGHTING SCHEMES. THE LEFT AND RIGHT VALUES REPRESENTS THE RESULTS OF SPDRFS AND SPUDRFS RESPECTIVELY.

Weighting Schemes CD DI	MO	MORPH		FGNET		BIWI		BU-3DFE		MPIIGaze	
weighting schemes	SP-DRFs	SPUDRFs									
Hard	1.85	1.78	2.68	2.66	1.24	0.76	0.94	0.84	4.58	4.45	
Linear	1.84	1.80	2.69	2.66	1.18	0.79	0.92	0.82	4.57	4.46	
Log	1.85	1.81	2.68	2.64	1.13	0.77	0.89	0.82	4.60	4.48	
Mixture	1.84	1.80	2.79	2.70	1.26	0.74	0.93	0.86	4.58	4.45	

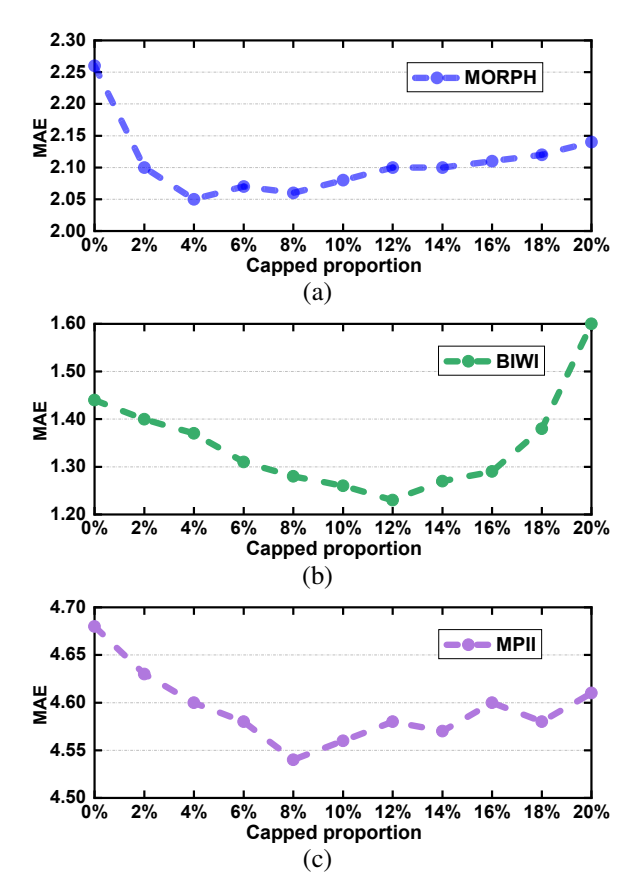


Fig. 8. The MAEs against variant capped proportions in our robust SPUDRFs on different datasets. (a) Morph II. (b) BIWI. (c) MPIIGaze.

Fig. 8 shows the MAEs against different capped proportions. When no example's likelihood is capped to 0, the corresponding MAE is large due to the presence of noise. As the caped proportion grows, the MAE gradually decreases. We observe when 10% samples are excluded, the MAEs almost achieve minimal values in Fig. 8(a), (b), and (c), which demonstrates robust SPUDRFs can handle noise examples effectively. When the capped proportion grows continuously, the MAE changes to increase. The underlying reason seems to be when the capped proportion becomes over 10%, the normal examples may begin to be discarded.

### F. Fairness Improvement

This section discusses how SPUDRFs improve regression fairness whereas SP-DRFs aggravate it.

To evaluate the regression fairness of DRFs, SP-DRFs and SPUDRFs, we calculated FAIR (defined in Sec. V) on

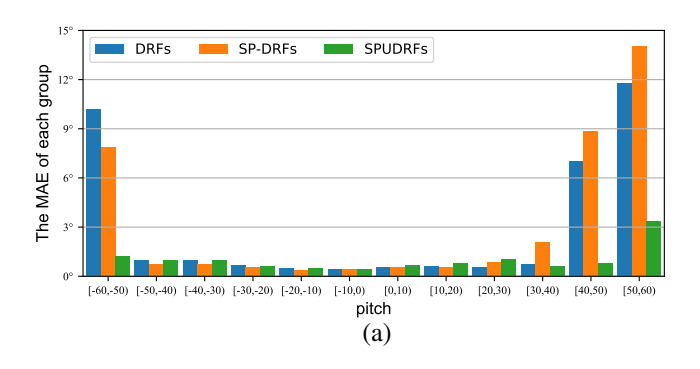
all aforementioned datasets. On Morph II, the age range is from 10 to 80, hence the entire data set was divided into 7 groups, *i.e.*, [10, 20], [20, 30], ..., [70, 80]. Similarly operation was conducted on FG-NET. On BIWI, the three directions (*i.e.*, pitch, yaw, and roll) were treated separately, and the interval of each group is 10°. On BU-3DFE, similar operation was done. On MPIIGaze, since the MAE was calculated as the angle between predicted gaze vector (*i.e.*, pitch and yaw) and ground truth vector, we used meshing method to divide groups. We set the group interval to be 5° on the above pitch and yaw directions, which produced a total number of 60 groups.

Table. IV shows the FAIR values on the Morph II, FG-NET, BIWI, BU3DFE and MPIIGaze datasets. The larger the FAIR is, the more fair the regression model is. We observe that SP-DRFs model is always inferior to DRFs on regression fairness, for example, 0.43 against 0.46 on BIWI. This demonstrates SP-DRFs tends to aggravate the bias of solutions, especially for obvious imbalanced data, such as BIWI. SPUDRFs has the capability to dramatically alleviate the unfairness of solutions, for example, on BIWI, the FAIR of SPUDRFs increases from 0.43 to 0.70. To the best of our knowledge, our work is the first to reveal the regression unfairness problem of DDMs in the scenario of SPL.

 ${\bf TABLE\ IV}$  Regression Fairness Evaluation on different datasets.

Methods	MORPH	FGNET	BIWI	BU-3DFE	MPIIGaze
DRFs	0.46	0.42	0.46	0.74	0.67
SP-DRFs	0.44	0.37	0.43	0.72	0.67
SPUDRFs	0.48	0.42	0.70	0.76	0.69

Visualizing the performance of SPUDRFs on different pose groups on BIWI is more intuitional as it exhibits how SPU-DRFs improve regression fairness. To this end, we plot the MAEs of different pose groups on the BIWI dataset in Fig. 9. The results show a consistent trend in the relative performance of DRFs, SP-DRFs and SPUDRFs. Firstly, SP-DRFs and SPU-DRFs have the capability to outperform DRFs on most groups in pitch and yaw direction. As discussed in Sec. III-B, this due to the self-paced regime for guiding DDMs to achieve better solutions. However, SP-DRFs has a tendency to achieve even worse solutions than DRFs in the region with scarce samples, for example,  $[30^{\circ}, 60^{\circ}]$  on pitch direction and  $[-70^{\circ}, -40^{\circ}]$ . This demonstrates the obvious drawback of the ranking and selecting way in original SPL, incurring more biased solutions. Finally, SPUDRFs exhibit significantly better performance in the regions with scarce samples, for example  $[-60^{\circ}, -50^{\circ}]$ and  $[30^{\circ}, 60^{\circ}]$  on pitch direction,  $[-70^{\circ}, -40^{\circ}]$  and  $[60^{\circ}, 70^{\circ}]$ 



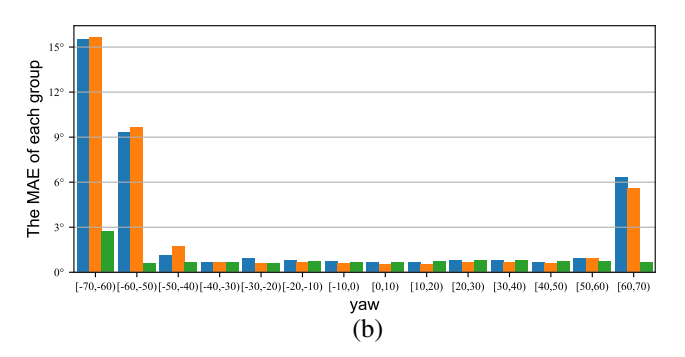


Fig. 9. The MAEs of different groups on BIWI dataset: (a) On the pitch direction, the pose range are divided into 12 groups. In the pose region with abundant training samples, both SP-DRFs and SPUDRFs can achieve better performance than DRFs, but in the range with scarce training samples (see Fig. 5), SPUDRFs, which considers underrepresented examples (i.e., ranking fairness), can significantly promote predictive accuracy. In the range of 30° to 60°, the MAE of SP-DRFs is even worse than DRFs. (b) On the yaw direction, we divide the pose range into 14 groups, and the similar phenomenon can be observed. This demonstrates the obvious drawback of the ranking and selecting scheme in original SPL—incurring biased solutions.

on yaw direction. This shows SPUDRFs obviously alleviate the unfairness of solutions.

### VII. DISCUSSION

In the above experiments, we have evaluated SPUDRFs against other methods in many scenarios: facial age estimation, head pose estimation and gaze estimation (Sec. VI-C). We also evaluated SPUDRFs with different weighting schemes, its extension with capped likelihood formulation, its performance improvement on regression fairness. On different tasks and datasets, SPUDRFs and SP-DRFs outperform other baseline methods. The advantage of considering ranking fairness in SPUDRFs is clearest on BIWI, where the leaf node coverage is obviously improved in SPUDRFs. On Morph II and BU-3DFE datasets, the performance promotion with considering ranking fairness in SPUDRFs is also relatively clear.

Learning DDMs by self-paced regime has some limitations. The most obvious one is, with leave-one-out setting, SP-DRFs performs only slightly superior than DRFs sometime, such as gaze estimation on MPIIGaze dataset. We speculate this is due to the heterogeneous data distribution between training set and test set in leave-one-out setting. Therefore, how self-paced regime can promote performance of DDMs on accuracy may mainly depend on the distribution divergence between training and test data.

### VIII. CONCLUSION

This paper explored how self-paced regime guided deep discriminative models (DDMs) to obtain more robust and less biased solutions on different computer vision tasks, *e.g.* facial age estimation, head pose estimation and gaze estimation. A novel self-paced paradigm, which considers ranking fairness, was proposed. Such a paradigm was incooperated with a typical DDM—deep regression forests (DRFs), and led to a new model, namely deep regression forests with consideration on underrepresented examples (SPUDRFs). Specifically, a new ranking scheme which jointly considers loss and predictive uncertainty was proposed in SPL. In addition, SPUDRFs with different weighting schemes, its extension with capped

likelihood formulation and its predictive performance on fairness were discussed. Extensive experiments on three well-known computer vision tasks demonstrated the efficacy of the proposed new self-paced paradigm. The future work will include exploring how to incorporate such a paradigm with other DDMs.

### ACKNOWLEDGMENT

The authors would like to thank Jiabei Zeng of Institute of Computing Technology, Chinese Academy on Sciences, for the useful discussion on the experiments on the MPIIGaze dataset. This work is partially founded by National Natural Science Fundation of China Nos. 61872068, 61806043, 61971106 and 62171111, China Postdoctoral Science Foundation No. 2017M623007, Sichuan Science and Technology program Nos. 2020YFG0288 and 2021YFG0366, and the Special Science Foundation of Quzhou No. 2020D013.

### REFERENCES

- S. Chen, C. Zhang, and M. Dong, "Deep age estimation: From classification to ranking," *IEEE Transactions on Multimedia*, vol. 20, no. 8, pp. 2209–2222, 2018.
- [2] C. Yan, C. Lang, W. Tao, X. Du, and Z. Chen, "Age estimation based on convolutional neural network," in *Pacific Rim Conference on Multimedia*, 2014, pp. 211–220.
- [3] S. Chen, C. Zhang, M. Dong, J. Le, and M. Rao, "Using Ranking-CNN for age estimation," in CVPR, 2017, pp. 742–751.
- [4] Y. Huang, L. Pan, Y. Zheng, and M. Xie, "Mixture of deep regression networks for head pose estimation," in *ICIP*. IEEE, 2018, pp. 4093– 4097
- [5] R. Rothe, R. Timofte, and L. Van Gool, "Deep expectation of real and apparent age from a single image without facial landmarks," *International Journal of Computer Vision*, vol. 126, no. 2-4, pp. 144– 157, 2018.
- [6] D. Huang, L. Han, and F. De la Torre, "Soft-margin mixture of regressions," in CVPR, 2017, pp. 4058–4066.
- [7] N. Ruiz, E. Chong, and J. M. Rehg, "Fine-grained head pose estimation without keypoints," in CVPR Workshops, 2018, pp. 2074–2083.
- [8] B.-B. Gao, H.-Y. Zhou, J. Wu, and X. Geng, "Age estimation using expectation of label distribution learning," in *IJCAI*, 2018, pp. 712–718.
- [9] O. M. Parkhi, A. Vedaldi, and A. Zisserman, "Deep face recognition," 2015.
- [10] Z. Niu, M. Zhou, L. Wang, X. Gao, and G. Hua, "Ordinal regression with multiple output CNN for age estimation," in CVPR, 2016, pp. 4920– 4928.

- [11] E. Agustsson, R. Timofte, and L. Van Gool, "Anchored regression networks applied to age estimation and super resolution," in *ICCV*, 2017, pp. 1643–1652.
- [12] Y. Cui, M. Jia, T.-Y. Lin, Y. Song, and S. Belongie, "Class-balanced loss based on effective number of samples," in CVPR, 2019, pp. 9268–9277.
- [13] S. Khan, M. Hayat, S. W. Zamir, J. Shen, and L. Shao, "Striking the right balance with uncertainty," in CVPR, 2019, pp. 103–112.
- [14] M. Ren, W. Zeng, B. Yang, and R. Urtasun, "Learning to reweight examples for robust deep learning," arXiv preprint arXiv:1803.09050, 2018.
- [15] M. P. Kumar, B. Packer, and D. Koller, "Self-paced learning for latent variable models," in NIPS, 2010, pp. 1189–1197.
- [16] L. Jiang, D. Meng, Q. Zhao, S. Shan, and A. G. Hauptmann, "Self-paced curriculum learning," in AAAI, 2015, pp. 2694–2700.
- [17] F. Ma, D. Meng, Q. Xie, Z. Li, and X. Dong, "Self-paced co-training," in *ICML*, 2017, pp. 2275–2284.
- [18] H. Li and M. Gong, "Self-paced convolutional neural networks," in IJCAI, 2017, pp. 2110–2116.
- [19] L. Pan, S. Ai, Y. Ren, and Z. Xu, "Self-paced deep regression forests with consideration on underrepresented examples," in ECCV, 2020.
- [20] D. Meng, Q. Zhao, and L. Jiang, "A theoretical understanding of self-paced learning," *Information Sciences*, vol. 414, pp. 319–328, 2017.
- [21] Z. Huang, Y. Ren, X. Pu, L. Pan, D. Yao, and G. Yu, "Dual self-paced multi-view clustering," *Neural Networks*, vol. 140, pp. 184–192, 2021.
- [22] Z. Huang, Y. Ren, X. Pu, and L. He, "Non-linear fusion for self-paced multi-view clustering," in ACM International Conference on Multimedia, 2021.
- [23] X. Guo, X. Liu, E. Zhu, X. Zhu, M. Li, X. Xu, and J. Yin, "Adaptive self-paced deep clustering with data augmentation," *IEEE Transactions* on Knowledge and Data Engineering, vol. 32, no. 9, pp. 1680–1693, 2019.
- [24] Y. Ren, P. Zhao, Y. Sheng, D. Yao, and Z. Xu, "Robust softmax regression for multi-class classification with self-paced learning," in Proceedings of the 26th International Joint Conference on Artificial Intelligence, 2017, pp. 2641–2647.
- [25] Y. Ren, X. Yan, Z. Hu, and Z. Xu, "Self-paced multi-task multi-view capped-norm clustering," in *International Conference on Neural Information Processing*. Springer, 2018, pp. 205–217.
- [26] L. Han, D. Zhang, D. Huang, X. Chang, J. Ren, S. Luo, and J. Han, "Self-paced mixture of regressions." in *IJCAI*, 2017, pp. 1816–1822.
- [27] J. Yang, X. Wu, J. Liang, X. Sun, M.-M. Cheng, P. L. Rosin, and L. Wang, "Self-paced balance learning for clinical skin disease recognition," *IEEE transactions on neural networks and learning systems*, 2019.
- [28] L. Jiang, D. Meng, S.-I. Yu, Z. Lan, S. Shan, and A. Hauptmann, "Self-paced learning with diversity," in NIPS, 2014, pp. 2078–2086.
- [29] W. Shen, Y. Guo, Y. Wang, K. Zhao, B. Wang, and A. Yuille, "Deep regression forests for age estimation," in CVPR, 2018, pp. 2304–2313.
- [30] W. Li, J. Lu, J. Feng, C. Xu, J. Zhou, and Q. Tian, "Bridgenet: A continuity-aware probabilistic network for age estimation," in CVPR, 2019, pp. 1145–1154.
- [31] Z. Deng, H. Liu, Y. Wang, C. Wang, Z. Yu, and X. Sun, "Pml: Progressive margin loss for long-tailed age classification," in CVPR, 2021, pp. 10503–10512.
- [32] G. Riegler, D. Ferstl, M. Rüther, and H. Bischof, "Hough networks for head pose estimation and facial feature localization," *Journal of Computer Vision*, vol. 101, no. 3, pp. 437–458, 2013.
- [33] Y. Wang, W. Liang, J. Shen, Y. Jia, and L.-F. Yu, "A deep coarse-to-fine network for head pose estimation from synthetic data," *Pattern Recognition*, vol. 94, pp. 196–206, 2019.
- [34] F. Kuhnke and J. Ostermann, "Deep head pose estimation using synthetic images and partial adversarial domain adaption for continuous label spaces," in *ICCV*, 2019, pp. 10164–10173.
- [35] X. Zhang, Y. Sugano, M. Fritz, and A. Bulling, "Appearance-based gaze estimation in the wild," in CVPR, 2015, pp. 4511–4520.
- [36] —, "It's written all over your face: Full-face appearance-based gaze estimation," in CVPR Workshops, 2017, pp. 51–60.
- [37] K. Krafka, A. Khosla, P. Kellnhofer, H. Kannan, S. Bhandarkar, W. Matusik, and A. Torralba, "Eye tracking for everyone," in CVPR, 2016, pp. 2176–2184.
- [38] T. Fischer, H. J. Chang, and Y. Demiris, "Rt-gene: Real-time eye gaze estimation in natural environments," in ECCV, 2018, pp. 334–352.
- [39] S. Park, A. Spurr, and O. Hilliges, "Deep pictorial gaze estimation," in ECCV, 2018, pp. 721–738.
- [40] S. Park, S. D. Mello, P. Molchanov, U. Iqbal, O. Hilliges, and J. Kautz, "Few-shot adaptive gaze estimation," in *ICCV*, 2019, pp. 9368–9377.

- [41] Y. Yu, G. Liu, and J.-M. Odobez, "Improving few-shot user-specific gaze adaptation via gaze redirection synthesis," in CVPR, 2019, pp. 11937– 11946.
- [42] Z. Chen and B. Shi, "Offset calibration for appearance-based gaze estimation via gaze decomposition," in *Proceedings of the IEEE/CVF Winter Conference on Applications of Computer Vision*, 2020, pp. 270–279
- [43] M. F. Huber, T. Bailey, H. Durrant-Whyte, and U. D. Hanebeck, "On entropy approximation for gaussian mixture random vectors," in *IEEE International Conference on Multisensor Fusion and Integration for Intelligent Systems*, 2008, pp. 181–188.
- [44] L. Jiang, D. Meng, T. Mitamura, and A. G. Hauptmann, "Easy samples first: Self-paced reranking for zero-example multimedia search," in ACM MM, 2014, pp. 547–556.
- [45] J. Fitzsimons, A. Al Ali, M. Osborne, and S. Roberts, "A general framework for fair regression," *Entropy*, vol. 21, no. 8, pp. 741–753, 2019
- [46] A. Agarwal, M. Dudík, and Z. S. Wu, "Fair regression: Quantitative definitions and reduction-based algorithms," in *ICML*, 2019, pp. 120– 129.
- [47] R. Berk, H. Heidari, S. Jabbari, M. Kearns, and A. Roth, "Fairness in criminal justice risk assessments: The state of the art," *Sociological Methods & Research*, vol. 50, no. 1, pp. 3–44, 2021.
- [48] J. Komiyama, A. Takeda, J. Honda, and H. Shimao, "Nonconvex optimization for regression with fairness constraints," in *ICML*, 2018, pp. 2737–2746.
- [49] M. B. Zafar, I. Valera, M. G. Rogriguez, and K. P. Gummadi, "Fairness constraints: Mechanisms for fair classification," in *Artificial Intelligence* and Statistics. PMLR, 2017, pp. 962–970.
- [50] K. Ricanek and T. Tesafaye, "Morph: A longitudinal image database of normal adult age-progression," in 7th International Conference on Automatic Face and Gesture Recognition (FGR06). IEEE, 2006, pp. 341–345.
- [51] G. Panis, A. Lanitis, N. Tsapatsoulis, and T. F. Cootes, "Overview of research on facial ageing using the fg-net ageing database," *Iet Biometrics*, vol. 5, no. 2, pp. 37–46, 2016.
- [52] G. Fanelli, M. Dantone, J. Gall, A. Fossati, and L. Van Gool, "Random forests for real time 3d face analysis," *International journal of computer* vision, vol. 101, no. 3, pp. 437–458, 2013.
- [53] L. Pan, J. M. Saragih, and W.-S. Chu, "Mixture of grouped regressors and its application to visual mapping," *Pattern Recognition*, vol. 53, pp. 184–194, 2016.
- [54] K. Zhang, Z. Zhang, Z. Li, and Y. Qiao, "Joint face detection and alignment using multi-task cascaded convolutional networks," *IEEE Signal Processing Letters*, vol. 23, no. 10, pp. 1499–1503, 2016.
- [55] K. Simonyan and A. Zisserman, "Very deep convolutional networks for large-scale image recognition," arXiv 1409.1556, 2014.
- [56] G. Guo, G. Mu, Y. Fu, and T. S. Huang, "Human age estimation using bio-inspired features," in CVPR, 2009, pp. 112–119.
- [57] I. Huerta, C. Fernández, and A. Prati, "Facial age estimation through the fusion of texture and local appearance descriptors," in ECCV, 2014, pp. 667–681.
- [58] K. Y. Chang, C. S. Chen, and Y. P. Hung, "Ordinal hyperplanes ranker with cost sensitivities for age estimation," in CVPR, 2011, pp. 585–592.
- [59] X. Geng, C. Yin, and Z.-H. Zhou, "Facial age estimation by learning from label distributions," *IEEE Transactions on Pattern Analysis and Machine Intelligence*, vol. 35, no. 10, pp. 2401–2412, 2013.
- [60] G. Guo, Y. Fu, C. Dyer, and T. Huang, "Image-based human age estimation by manifold learning and locally adjusted robust regression," *IEEE Transactions on Image Processing*, vol. 17, no. 7, pp. 1178–1188, 2008
- [61] Z. Yu and D. Y. Yeung, "Multi-task warped gaussian process for personalized age estimation," in CVPR, 2010, pp. 2622–2629.
- [62] H. Han, C. Otto, X. Liu, and A. K. Jain, "Demographic estimation from face images: Human vs. machine performance," *IEEE Transactions on Pattern Analysis and Machine Intelligence*, vol. 37, no. 6, pp. 1148–1161, 2015.
- [63] K. Luu, K. Seshadri, M. Savvides, T. D. Bui, and C. Y. Suen, "Contourlet appearance model for facial age estimation," in *International Joint Conference on Biometrics*, 2013, pp. 1–8.
- [64] H. Drucker, C. J. Burges, L. Kaufman, A. J. Smola, and V. Vapnik, "Support vector regression machines," in NIPS, 1997, pp. 155–161.
- [65] A. Liaw, M. Wiener et al., "Classification and regression by randomforest," R news, vol. 2, no. 3, pp. 18–22, 2002.
- [66] M. Al Haj, J. Gonzalez, and L. S. Davis, "On partial least squares in head pose estimation: How to simultaneously deal with misalignment," in CVPR, 2012, pp. 2602–2609.

- [67] G. E. Hinton and R. R. Salakhutdinov, "Reducing the dimensionality of data with neural networks," *science*, vol. 313, no. 5786, pp. 504–507, 2006
- [68] T. Guo, H. Zhang, B. Yoo, Y. Liu, Y. Kwak, and J.-J. Han, "Order regularization on ordinal loss for head pose, age and gaze estimation," in AAAI, vol. 35, no. 2, 2021, pp. 1496–1504.
- [69] X. Zhang, Y. Sugano, M. Fritz, and A. Bulling, "Mpiigaze: Real-world dataset and deep appearance-based gaze estimation," *IEEE transactions* on Pattern Analysis and Machine Intelligence, vol. 41, no. 1, pp. 162– 175, 2017.
- [70] Y. Xiong, H. J. Kim, and V. Singh, "Mixed effects neural networks (menets) with applications to gaze estimation," in CVPR, 2019, pp. 7743–7752.



Lili Pan received her B.Eng. degree in Electronic Engineering, as well as her M.Eng. and Ph.D. degrees in Information Engineering from University of Electronic Science and Technology of China (UESTC), China, in 2004, 2007, and 2012, respectively. From 2009 to 2011, she visited the Robotics Institute of Carnegie Mellon University, USA. She joined the Department of Information Engineering, UESTC, as a lecturer in 2012. She is currently an associate professor at UESTC. Her research interests include deep discriminative models, generative

adversarial networks and interpretable machine learning.



Mingming Meng received his B.Eng. degree from University of Electronic Science and Technology of China (UESTC), China, in 2019. He Currently pursues for his master degree in Information Engineering at UESTC. His research interests include deep discriminative model, fairness in deep models and generative adversarial networks.



Yali Zheng received her PhD from Chongqing University in 2012, and joined the School of Automation Engineering, University of Electronic Science and Technology of China in 2013. From 2008 to 2011, she visited he Robotics Institute of Carnegie Melon University, USA. Her research interests include machine learning, pattern recognition and computer vision, especially on graph matching, deep learning, and their applications in industry fields.



Yazhou Ren is currently an associate professor with the School of Computer Science and Engineering, University of Electronic Science and Technology of China, Chengdu, China. He received the B.Sc. degree in information and computation science and the Ph.D. degree in computer science from the South China University of Technology, Guangzhou, China, in 2009 and 2014, respectively. He visited the Data Mining Laboratory, George Mason University, USA, from 2012 to 2014. He has published more than 50 peer-reviewed research articles. His current research

interests include clustering, self-paced learning, and multi-view learning.



Zenglin Xu received the Ph.D. degree in computer science and engineering from the Chinese University of Hong Kong. He is currently a full professor in Harbin Institute of Technology, Shenzhen, and also affiliated with Peng Cheng Lab. He has been working at Michigan State University, Cluster of Excellence at Saarland University and Max Planck Institute for Informatics, Purdue University, and University of Electronic Science & Technology of China. Dr. Xu's research interests include machine learning and its applications in computer vision,

natural language processing, and health informatics. He currently serves as an associate editor to Neural Networks and Neurocomputing. He is the recipient of the outstanding student paper honorable mention of AAAI 2015, the best student paper runner up of ACML 2016, and the 2016 young researcher award from APNNS.